JOURNAL OF MATERIALS SCIENCE 31 (1996) 137–143

Quantitative phase analysis of metastable structure in a laser melted Fe–C alloy

Part I *Structural analysis of single melted tracks by SEM and TEM*

N. ZÁRUBOVÁ, P. WOLF, J. ČERMÁK, M. ČERŇANSKÝ
Institute of Physics, Academy of Sciences of the Czech Republic, Na Slovance 2, CZ-180 40 Praha 8, Czech Republic

Pure Fe–3.5 wt % C alloy was surface melted using a cw CO_2 laser and the microstructure of the laser tracks was investigated by scanning and transmission electron microscopy. Structure of the melted zones consisted of dendrites of partially transformed primary austenite and of very fine lamellar ledeburite. The secondary dendrite arm spacings were indicative of a cooling rate of $\sim 10^5\ K\,s^{-1}$, in good accord with calculations based on the model of a moving Gaussian beam. Using methods of quantitative metallography the volume fraction of dendrites within the melted zone and the volume fractions of the carbide and ferrite phases in the decomposed ledeburite were estimated. These data were combined with the results of a quantitative X-ray diffraction phase analysis (see Part II) and compared with the equilibrium phase diagram. It was found that the volume fraction of dendrites was near the equilibrium value while the volume content of cementite in the rapidly solidified structures was considerably higher than predicted from the equilibrium phase diagram.

1. Introduction

Similarly to other technologies of rapid solidification, laser surface melting offers a unique method of producing novel, often high performance materials. High power densities of the laser beam and extreme heating and cooling rates during treatment result in a great variety of metastable phases forming surface layers of significant physical and chemical properties. Because of their technological importance, Fe–C based alloys, cast irons as well as steels, represent a group of materials frequently exposed to the laser surface treatment (references concerning cast irons were summarized in our recent paper [1]). The pure binary Fe–C system was investigated in detail by Walker and co-workers [2, 3] who used optical and electron microscopy as well as X-ray diffraction to identify the structural components in laser alloyed surface layers. Quite recently Amulyavichyus *et al.* [4] published their study on Fe–C surface layers produced by introducing carbon into technical iron by means of a pulsed laser.

Although the structure of the laser modified layers has been treated rather extensively, there is a lack of direct quantitative information on metastable structures encountered in these rapidly solidified materials. In the present study X-ray diffraction and metallographic observations by electron microscopy have been combined to perform a quantitative structural analysis of a laser melted Fe–3.5 wt % C alloy. The Fe–C alloys represent a simple binary system with well known transformation kinetics for cooling rates up to about $10^3\ K\,s^{-1}$. On the side of extreme cooling rates, several authors [5–11] investigated various Fe–C alloys subjected to melt spinning or splat quenching where the cooling rates in excess of $10^6\ K\,s^{-1}$ resulted in highly metastable structures including an amorphous phase. The quenching rates attained in our experiments were located between the two limits. The results of our study are presented in two parts. In Part I metallographic investigations of single tracks by scanning and transmission electron microscopy are described, the results are correlated with X-ray diffraction data and some deviations from the equilibrium phase diagram are discussed. In Part II the method of quantitative phase analysis by X-ray diffraction is described in detail and results obtained by this method on superimposed laser tracks are presented and discussed.

2. Experimental techniques

The experiments were performed on a pure hypoeutectic vacuum melted and cast Fe–C alloy. According to a chemical analysis the carbon concentration was 3.5 wt %. The starting microstructure consisted of pearlite and ferrite/cementite eutectic (decomposed ledeburite). Specimens $10 \times 20 \times 40\ mm^3$ were finely ground and surface melted using a continuous CO_2 laser operated at a nominal power of 1500 W.

0022–2461

A defocused beam was used for the experiments. The irradiation was made under Ar shielding, and the scanning speed, v, of the beam over the specimen surface varied from 4 to 65 cm s^{-1}.

The microstructural investigations by optical and scanning electron microscopy (SEM) were made on nital etched cross-sections of the melted tracks and on the longitudinal sections perpendicular to the specimen surface. For transmission electron microscopy (TEM) 3 or 2.3 mm discs were cut parallel to the top surface of the melted track. After grinding the discs were thinned by electropolishing in a solution of perchloric acid in methanol at -40°C and observed at 100 and 200 kV. Since the laser melted tracks were narrow and cracked, preparation of the TEM foils was extremely difficult and we succeeded in preparing foils only for the lowest scanning speed, $v = 4$ cm s^{-1}.

3. Mathematical modelling of the temperature distribution

In order to get an estimation of the temperature regime during irradiation, the model of a moving Gaussian beam published by Cline and Anthony [12] was adopted. In this model the beam moves at a constant velocity on the surface of the specimen taken as the infinite half-space. All physical characteristics are considered to be temperature independent, and the latent heat of melting is not taken into account. In the stationary state the temperature distribution is given by

$$T(X,Y,Z) = \frac{P}{K\pi^{3/2}R}\int_0^\infty \exp\left\{-\frac{(X+\rho\mu^2)^2+Y^2}{1+\mu^2} - \frac{Z^2}{\mu^2}\right\}\frac{d\mu}{1+\mu^2} \quad (1)$$

where X, Y, Z = dimensionless coordinates ($X = x/R$, etc.), P = total incident power, K = thermal conductivity, $R = (P/\pi I(0))^{1/2}$ = beam radius, $I(0)$ = power density in the centre of the Gaussian beam, $\rho = Rv/4\kappa$, κ = thermal diffusivity, and v = scanning velocity. The temperature distribution during the thermal cycle was obtained by numeric solution to Equation 1. Since the beam radius and the absorbed power could not be measured directly, the values of R and P were estimated by fitting the track geometry. As seen from Fig. 1, the calculations of T fit well the depth and width of the melted zone as functions of v when taking the melting temperature $T_M = T_E = 1150$°C (the eutectic temperature), $K = 0.293$ W cm^{-1} K^{-1}, $\kappa = 0.043$ cm^2 s^{-1}, $P = 220$ W (15 % effective absorptivity) and $R = 0.3$ mm. Equation 1 was used also for an estimation of the cooling rate and of the effect of subsequent annealing of the already melted region in the case of superimposed passes (see Part II).

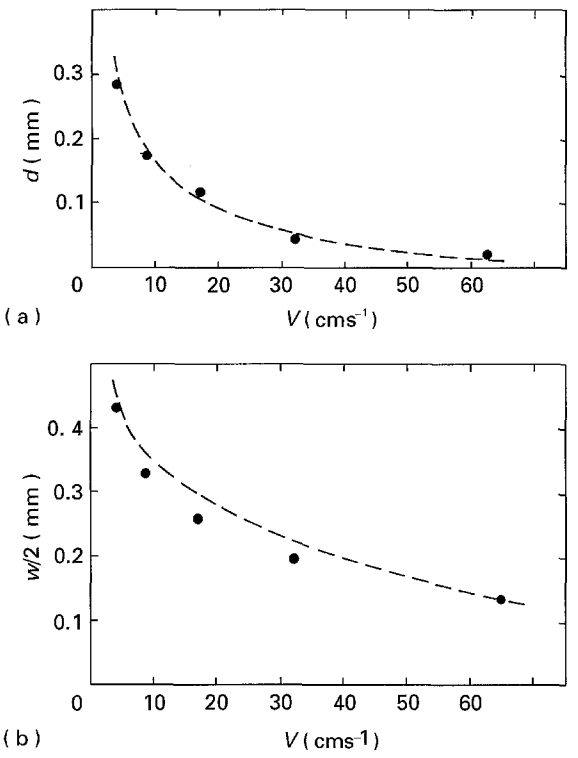

Figure 1 Depth (a) and width (b) of the melted zone as functions of the scanning speed. • measured data, - - - solution to Equation 1.

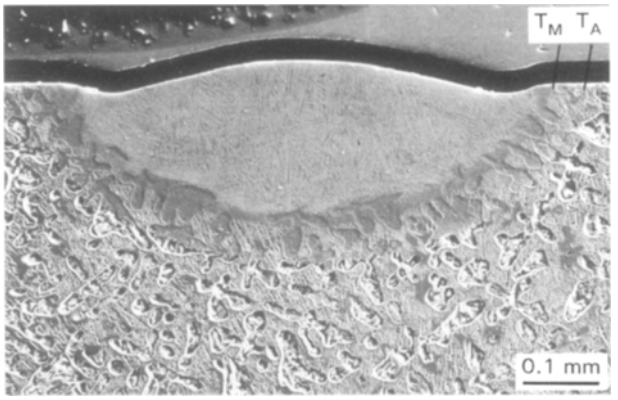

Figure 2 Cross-sectional view of a laser surface melted specimen, $v = 8.5$ cm s^{-1}. T_M and T_A are the phase boundaries corresponding to the melting and austenitization temperatures, respectively.

4. Experimental results

4.1. Structure of the melted zone

A cross-section of the melted track is shown in Fig. 2. Due to the defocused beam the tracks were rather shallow. For the lower scanning speeds, $v = 4$, 8.5 and 17 cm s^{-1}, the original structure was completely remelted and convection in the melt pool was obviously sufficient to produce a homogeneous melt.

Typical examples of the microstructure in the melted zone are shown in Figs 3 and 4. The structure is formed by dendrites of partially transformed primary austenite, and by very fine eutectic (decomposed ledeburite). Martensite needles are well distinguishable in the dendrite interior (see Figs 3c and 4a). The TEM examination revealed, however, that beside martensitic transformation the austenite decomposed

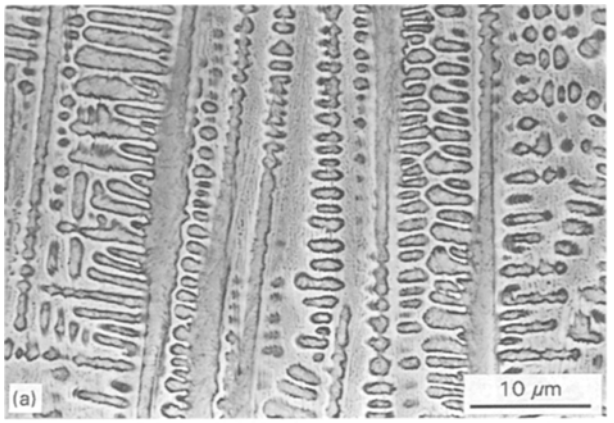

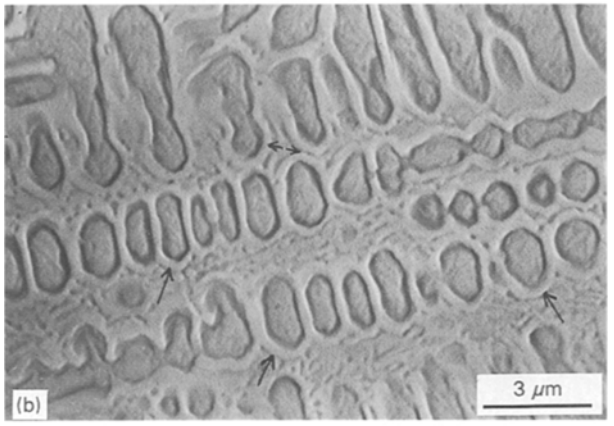

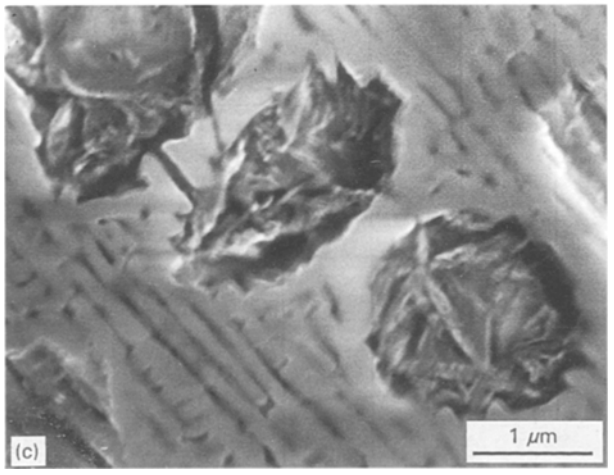

Figure 3 SEM micrographs of the structure in the melted zone. (a) and (b) Dendrites of partly transformed primary austenite, $v = 4\ \mathrm{cm\,s^{-1}}$; arrows indicate carbide layers encircling the dendrite arms. (c) A detail of the same structure for $v = 8.5\ \mathrm{cm\,s^{-1}}$; martensite needles are well visible inside the dendrites; the lamellar eutectic (ledeburite) is formed by ferrite (dark) and cementite (light).

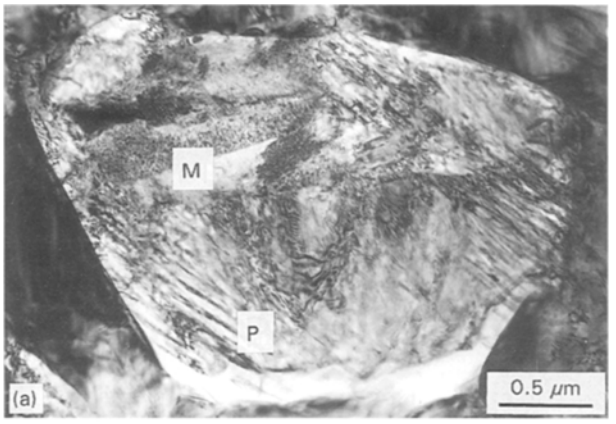

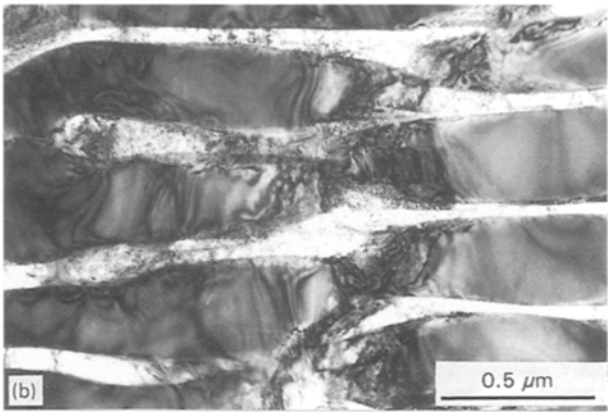

Figure 4 TEM micrographs of the structure in the melted zone, $v = 4\ \mathrm{cm\,s^{-1}}$. (a) Primary austenite transformed partly to martensite (M), partly to pearlite (P). (b) Lamellar eutectic (ledeburite) consisting of ferrite (light) and cementite (dark).

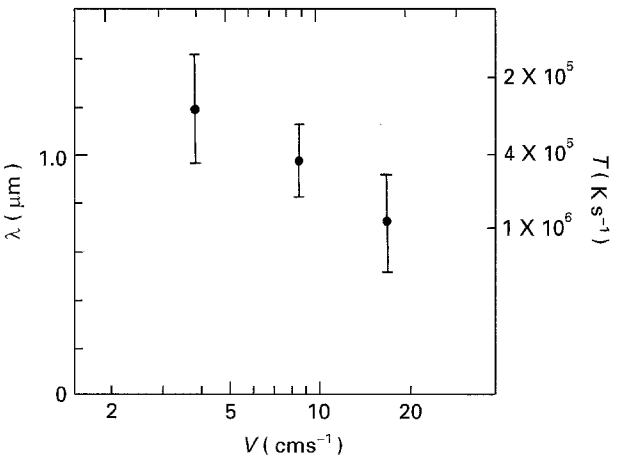

Figure 5 Secondary dendrite arm spacing, λ, as a function of the scanning speed. The right-hand scale indicates the cooling rate, $\dot{T}$, calculated according to [13].

locally into extremely fine pearlite, with lamellar spacings ~40 nm (see Fig. 4a). The secondary dendrite arms are encircled by relatively thick, up to ~0.5 μm, layers of carbide, as clearly visible in Fig. 3b and c.

At the higher scanning speeds, $v = 32$ and $65\ \mathrm{cm\,s^{-1}}$, formation of the secondary dendrite arms is strongly limited. However, remnants of the parent structure (substrate) were visible within the melted zone so that the melt was evidently inhomogeneous. For this reason the microstructure of the melted zone was not studied in detail for these scanning speeds.

4.2. Secondary dendrite arm spacing

The secondary dendrite arm spacings, λ commonly taken as a quantitative measure of the cooling rate $\dot{T}$ during solidification, were measured for $v = 4$, 8.5 and $17\ \mathrm{cm\,s^{-1}}$ in the middle part of the melted zones. The values of λ (see Fig. 5) are comparable with the λ values observed by Vogt and Frommeyer [13] in melt spun ribbons of Fe–3.2 wt % C. These authors correlated the secondary arm spacings with the cooling rates estimated directly from pyrometer measurements during melt spinning. Their results fit well the

exponential relation $\lambda = c\dot{T}^{-a}$, with empirical constants $c = 170$ and $a = 0.4$ (if λ is given in μm and $\dot{T}$ in $K\,s^{-1}$). The right-hand scale in Fig. 5 indicates the cooling rates estimated for our structures taking the same constants c and a. The values of $\dot{T}$ in the upper part of the melted zone calculated from the heat transfer model (Section 3) are 0.5×10^5, 1×10^5 and 2.5×10^5 $K\,s^{-1}$ for $v = 4$, 8.5 and 17 $cm\,s^{-1}$, respectively. The agreement between the experimental and the calculated values is quite good if we take into account the approximations made in the mathematical model and the uncertainty in the constants a and c (e.g. due to higher carbon content in our alloy).

4.3. Volume fraction of dendrites

In order to get a quantity which could be related to the quantities obtained by X-ray diffraction, the volume fraction of dendrites in the melted zone was determined using the point counting method [14].

The volume of dendrites was measured without the carbide layers encircling the dendrite arms. The measurements were made on SEM micrographs (magnification 2000) and about 10 photos were taken to get one point in Fig. 6. Within the experimental scatter the volume fraction of dendrites, Ω, was independent of the position within the melted zone. As is apparent from Fig. 6, Ω also remains constant with increasing scanning rate, and the values of Ω found for single tracks agree very well with the similar measurements on overlapping passes (see Part II). The mean volume fraction of dendrites in the melted zone was ~0.33.

4.4. Structure of the eutectic

Except for the thick carbide layers around the dendrites, the interdendritic regions consist of a very fine lamellar eutectic (ledeburite) at room temperature (Figs 3c and 4b). No martensite needles were discernible within the metallic lamellae by TEM. This fact, together with the results of X-ray diffraction (Part II) indicates that the original austenite parts of the eutectic transformed to ferrite on cooling.

With respect to the X-ray analysis it was highly desirable to obtain from the metallographic observations some quantitative information about the amount of carbide in the eutectic. Though the lamellar structure of the eutectic could be recognized by SEM for all scanning speeds, the quantitative measurements had to be made on TEM micrographs. Consequently, only data for $v = 4$ $cm\,s^{-1}$ are available. In the TEM micrographs the carbide lamellae may screen the ferrite parts if the lamellar structure is oblique to the foil plane. For this reason the foils were tilted in the microscope so that the maximum width of the ferrite strips was achieved. The volume fraction of the ferrite in the eutectic, as estimated by the point counting method [14] from about twenty micrographs (magnified ≃25 000), varied on individual pictures from 0.11 to 0.33. On the average, the width ratio of the ferrite–carbide phases in the lamellar ledeburite was estimated to be about 1:5. For $v = 4$ $cm\,s^{-1}$ the lamellar spacing was typically 0.2 to 0.3 μm.

4.5. Structure of the "mushy zone"

Fig. 7 shows a detail of the transition region between the melted and austenitized zones (the so called "mushy zone"). In the upper part of the micrograph where the peak temperature exceeded the liquidus temperature (line L) the material was completely remelted. Between the liquidus and solidus (line S) only the eutectic part of the initial structure was melted while the original pearlitic grains remained undissolved. During heating pearlite transformed to austenite. The outer parts of the austenite grains were strongly carbon enriched from the surrounding melt of the eutectic composition. Consequently, these outer parts remained nearly fully austenitic after cooling whereas in the grain interiors austenite transformed to martensite.

Below the solidus temperature $S \simeq T_E = 1150°C$, austenitization and subsequent transformation to martensite occurred during the thermal cycle. The outer boundary of the austenitized zone T_A, marked in Fig. 2, coincides for $v = 4$ and 8.5 $cm\,s^{-1}$ quite well with the isotherm $A_{C1} = 723°C$ calculated from Equation 1. For $v = 17$ $cm\,s^{-1}$ the measured width of the

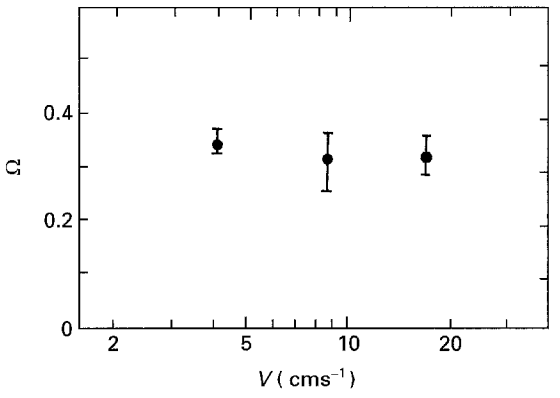

Figure 6 Volume fraction of dendrites as a function of the scanning speed.

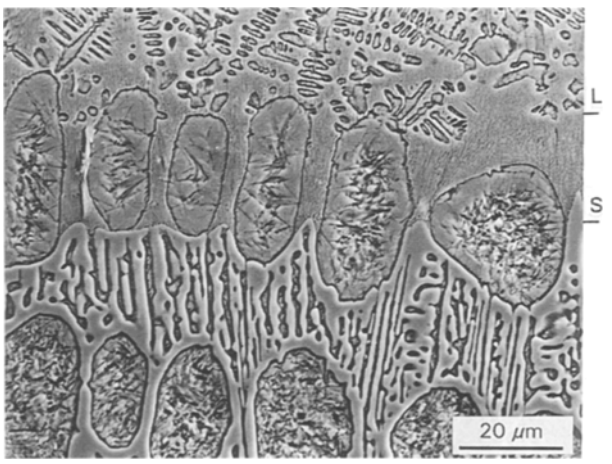

Figure 7 Detail of the "mushy zone"–transition between the melted and austenitized zones, $v = 8.5$ $cm\,s^{-1}$, SEM. *L* ... liquidus, *S* ... solidus $\simeq T_E = 1150°C$.

austenitized zone is smaller than that given by the calculated A_{C1} isotherm, and the austenitization temperature T_A seems to be shifted to the temperature $A_{C3} = 900°C$. Such a shift of T_A has been described for laser annealed plain carbon steel in [15], and for laser melted grey cast iron in [1] where the kinetics of austenitization at high heating rates were discussed in detail.

5. Discussion

In the preceding section microstructure of the melted zone was described and some quantitative data were obtained using methods of quantitative metallography. In Part II of this paper results of a quantitative X-ray diffraction phase analysis are presented. The X-ray measurements were taken on overlapping passes, nevertheless an extrapolation to non-interfering tracks was attempted so that the X-ray data and the metallographic data on the single tracks could be correlated. Before doing that, it is necessary to realize the principal differences and inherent errors in data obtained by the two essentially different methods. Optical and electron metallography identifies the shape and area of plane geometrical figures observed on metallographic sections suitably etched before examination. Because of etching artifacts which may distort the quantitative results, evaluation of these figures depends critically on the applied etchant and the experience of the observer. X-ray diffraction identifies crystallographic units disregarding their shape, size and distribution in the crystal aggregate. The X-ray diffraction patterns include intensities from all, more or less finely dispersed, particles of the same crystallographic structure throughout the whole irradiated volume of the sample. Quantitative results based on measurements of only intensity of the diffraction lines may be distorted by the real structure of the material (preferred orientation, defects, inhomogeneities, strains, particle size, etc.) of the polycrystalline aggregate but do not depend on the observer.

The structural constituents of our Fe–C alloy after laser melting were α-Fe (martensite and ferrite), γ-Fe (retained austenite) and carbide (cementite). The volume fractions of these phases estimated from the X-ray diffraction data are presented in Table I, together with the volume fraction of dendrites and the width ratio of the ferrite–carbide phases in the lamellar eutectic (ledeburite). In the same table corresponding equilibrium quantities are summarized as determined from the metastable Fe–Fe_3C phase diagram using the lever rule. The equilibrium data are given for the eutectic temperature $T_E = 1150°C$ and for room temperature. Since the densities of the relevant phases are very close to each other (7.88, 7.65 and 7.70 g cm^{-3} for α-Fe, γ-Fe and Fe_3C, respectively) and the accuracy of the measured quantities is rather limited, the difference between the volume and mass percentages was neglected.

The most remarkable result of the X-ray analysis is the high amount of carbide and, correspondingly, low amount of the metallic (α + γ) phase. In the following we shall compare these findings with the metallographic observations. From Table I it is evident that the volume fraction of primary austenite crystallizing from the melt in the form of dendrites was near the equilibrium value even though the cooling rates during solidification might have been as high as 10^5 K s^{-1}. On further cooling the primary austenite partly transformed. The SEM and TEM micrographs indicate that the γ-Fe (retained austenite) identified by X-ray diffraction often forms the central parts of the dendrites where the diffusion distances for carbon were too long and, thus, the martensite transformation was suppressed. The data in Table I indicate that about fifty per cent of the primary austenite was retained upon cooling to room temperature.

We shall now consider the complementary, i.e. the ledeburitic part of the solidified structure. The carbon atoms rejected from the solidifying primary austenite obviously did not have enough time to diffuse and formed thick carbide shells around the dendrites. We may suppose that during cooling from the eutectic temperature some secondary cemetite segregated at those carbide layers. A rough estimation shows that the volume fraction of these carbide shells may be comparable with the volume fraction of dendrites, i.e. as high as ~0.3. The other part of the interdendritic

TABLE I Phase composition of metastable Fe–3.5 wt % C alloy

	After laser treatment				Equilibrium values	
V (cm s^{-1})	4	8.5	17	methods	1150 °C	20 °C
Volume fraction of						
α–Fe	–	0.23	0.21	X-ray diffraction, see Part II	–	0.47
γ–Fe	–	0.16	0.19		0.68	–
Cementite	–	0.61	0.60		0.32	0.53
Dendrities	0.34	0.32	0.33	metallography, this Part (I)	0.36[a]	0.28[b]
Width ratio of ferrite/cementite lamellae in ledeburite	1:5	–	–		1:1	1:2

[a]Primary austenite.
[b]Pearlite; all secondary cementite is supposed to have segregated on the boundaries of the austenite grains; all tertiary cementite is supposed to have segregated within the austenite grains.

structure is formed by lamellar eutectic. The microscopic examinations indicate that in the regions of the lamellar eutectic the ratio of ferrite to cementite is roughly 1:5 in contrast to the equilibrium value 1:2. It means that the lamellar eutectic is considerably richer in carbide than expected for the equilibrium conditions. Although the entire volume occupied by carbide was not determined from the micrographs, the conclusions of the metallographic examination seem to be at least consistent with the X-ray measurements, and confirmed the rather high amount of carbide in our laser treated samples.

The high amount of carbide in the melted zone, ~ 0.6 of the entire volume, indicates that the cementite can not be the stoichiometric Fe_3C. For the composition of the alloy Fe–3.5 wt % C, the content of Fe_3C could be a maximum of ~ 0.53 (the equilibrium value). In fact, the carbon content available for carbide formation is even lower in the rapidly quenched structure because some of the carbon atoms remained dissolved in the martensite and retained austenite forming dendrites. The entire amount of this "trapped" carbon can be very roughly estimated from the fact that about one half of the primary austenite transformed to the martensite on cooling to room temperature. It is known that the martensite start (M_s) and martensite finish (M_f) temperatures are strongly dependent on the carbon content, and from the data published, e.g. in [16], we may deduce that in our case the average concentration of carbon in the dendrites should be about 1.5 wt %. Since the volume ratio of dendrites is ~ 0.33 (metallography), we can estimate that the entire amount of carbon retained in them is ~ 0.5 wt %. In this way the carbon content available for carbide formation was only ~ 3.0 wt % and the corresponding volume content of Fe_3C, as determined using the lever rule, would be about 0.45. The measured volume fraction of the carbide is, however, about 0.6 (X-ray diffraction), which indicates that its average composition should be close to Fe_4C.

Let us now compare our results with the data published so far in the literature. Transformation kinetics of the Fe–C system are relatively well known for cooling rates up to about 10^3 K s^{-1}, and the corresponding time–temperature–transformation (TTT) diagrams or continuous cooling–transformation (CCT) diagrams may be found in classical books on metallurgy, e.g. [16]. The system, however, has been the subject of considerable interest at higher cooling rates as well.

Walker and co-workers [2, 3] introduced carbon into pure iron by means of laser surface alloying. The structure in the melted zone was formed by dendrites and lamellar eutectic in the case of the hypoeutectic composition, and by pro-eutectic cementite and lamellar eutectic in the hypereutectic alloys. The cooling rates from the melt were estimated to be $\sim 10^4$ K s^{-1}. Under these conditions the γ-dendrites partly transformed to martensite while the structural constituents of the eutectic part were Fe_3C and ferrite, as found by electron and X-ray diffraction. In [3] the authors state that in the most perfectly lamellar regions of the eutectic the width ratio of ferrite–carbide phases was close to the equilibrium value 1:2. However, in [2], on the basis of metallographic observations, they admit that the volume fraction of Fe_3C in the eutectic might be greater than expected from equilibrium considerations.

Similar structural analysis was performed by Eiselstein *et al.* [17] on rapidly solidified white cast iron powders with 2.4 and 3.0 wt % C. The quenching rates reached in this study were greater than 10^5 K s^{-1} and varied with the particle size. The microstructure consisted of dendrites or cells of retained austenite (with only a small amount of martensite), and of ledeburite representing a mixture of retained austenite and carbides. The volume fraction of primary austenite was higher in coarser particles than in fine powders, which was interpreted as a direct consequence of the slower cooling rate of coarse particles compared to fine particles. However, a quantitative measurement of the volume fraction of the structural constituents was obviously not performed.

A comparable cooling rate, $\sim 10^5$ K s^{-1}, was attained also by Amulyavichyus *et al.* [4] who introduced carbon into iron by means of a pulsed laser. The authors applied optical microscopy, microprobe measurements, X-ray diffraction and Mössbauer spectroscopy to analyse the alloyed zones and revealed that under rapid laser quenching conditions non-stoichiometric carbides can form. They identified carbide structures of composition $Fe_{1-x}C_x$ with $0.19 \leqslant x \leqslant 0.32$ corresponding to the composition range from $Fe_{4.3}C$ to $Fe_{2.1}C$.

Ruhl and Cohen [5, 6] were the first to investigate the iron–carbon alloys after quenching from liquid state by splat cooling. The cooling rates attained in their experiments ranged from 10^5 to 10^8 K s^{-1}. They reported for the first time formation of the ε-phase which was identified as an interstitial solid solution of carbon in h c p iron and has been explored by several investigators since then [8–11]. Formation of an amorphous structure in splat cooled Fe–C alloys was reported for example in papers [7, 8].

The cooling rates $\sim 10^5$ K s^{-1} attained in our experiments are comparable with those encountered in [2–4, 17] and also the observed microstructure is, at least qualitatively, in good accord with the microstructures described by these authors. However, some differences and new results should be stressed. The quantitative measurements show clearly that the carbide (cementite) content in the laser melted zone is considerably higher than would be expected for the equilibrium conditions. Consequently, the cementite must be of non-stoichiometric composition, rather Fe_4C than Fe_3C, which is in good agreement with [4]. Since the carbide content is too high, the amount of the metallic components (austenite, martensite, ferrite) is correspondingly low. Our measurements, however, show that the volume fraction of primary austenite crystallizing from the melt in the form of dendrites was close to the equilibrium value and approximately the same for all investigated scanning speeds. Thus, we did not confirm the result by Eiselstein *et al.* [17] who observed a decreasing amount of primary austenite with increasing cooling rate. The interval of cooling

rates covered by our experiments was perhaps too small to yield a measurable effect. On the other hand, the eutectic part of the structure proved to contain too much carbide and, thus, to be far from equilibrium. A similar result was already mentioned by Walker *et al.* [2], nevertheless very vaguely and marginally whereas we can state this fact positively and document it quantitatively.

6. Conclusions

The microstructure of laser melted Fe–3.5 wt % C alloy has been investigated by scanning and transmission electron microscopy. The main results are as follows:

1. Structure of the melted zones was formed by dendrites of primary austenite partly transformed to martensite and extremely fine pearlite, and by very fine ferrite/cementite eutectic (decomposed ledeburite). From the secondary dendrite arm spacings the cooling rate during solidification was estimated to be $\sim 10^5$ K s^{-1}.
2. The volume fraction of dendrites was about 0.33, irrespective of the position in the melted zone and of the scanning speed. This value corresponds approximately to the equilibrium value.
3. The width ratio of the ferrite–carbide phases in the ledeburite was $\sim$ 1:5, in contrast to the equilibrium value 1:2.
4. The metallographic observations confirm the very high amount of cementite found in the resolidified structure by quantitative X-ray diffraction phase analysis (see Part II). The volume fraction of the carbide was estimated to be ~ 0.60, which indicates that the composition of the rapidly solidified cementite was Fe_4C rather than Fe_3C.

Acknowledgements

The authors are grateful to Dr J. Lašek for valuable comments on the manuscript. The work was supported by the Grant Agency of the Academy of Sciences of the Czech Republic under grant No. 11047 and this support is gratefully acknowledged.

References

1. N. ZÁRUBOVÁ, V. KRAUS and J. ČERMÁK, *J. Mater. Sci.* **27** (1992) 3487.
2. A. WALKER, D.R.F. WEST and W.M. STEEN, *Met. Technol.* **11** (1984) 399.
3. A. WALKER, H.M. FLOWER and D.R.F. WEST, *J. Mater. Sci.* **20** (1985) 989.
4. A. AMULYAVICHYUS, M. BALCHYUNENE, S. GRIGALYUNAS and B. PETRETIS, *Fiz. Met. Met.* **76** (1994) 94.
5. R.C. RUHL and M. COHEN, *Acta Metall.* **15** (1967) 159.
6. *Idem, Trans. AIME* **245** (1969) 241.
7. P.H. SHINGU, K. KOBAYASHI and R. OZAKI, *Scripta Metall.* **8** (1974) 1317.
8. P.G. BOSWELL and G.A. CHADWICK, *J. Mater. Sci.* **11** (1976) 2287.
9. J.M. DUBOIS and G. LE CAER, *Acta Metall.* **25** (1977) 609.
10. I. SCHMIDT and E. HORNBOGEN, *Z. Metallkde.* **69** (1978) 221.
11. I.R. SARE, *J. Mater. Sci.* **16** (1981) 3470.
12. H.E. CLINE and T.R. ANTHONY, *J. Appl. Phys.* **48** (1977) 3895.
13. E. VOGT and G. FROMMEYER, *Z. Metallkde.* **78** (1987) 262.
14. E.R. WEIBEL, in "Stereological Methods", Vol. 1 (Academic Press, London 1979).
15. A. LUFT, D. LEPSKI, B. BRENNER and W. REITZENSTEIN, *Wissenschaftliche Berichte des ZFW Dresden* **36** (1988) 111.
16. H. SCHUMANN, in "Metallographie", 11. Auflage (VEB Deutscher Verlag für Grundstoffindustrie, Leipzig, 1983) p. 357.
17. L.E. EISELSTEIN, O.A. RUANO and O.D. SHERBY, *J. Mater. Sci.* **18** (1983) 483.

Received 6 September 1994
and accepted 17 July 1995